

Supplementary Material

Fully printable Sb₂S₃-based mesoscopic triple-stack solar cells: The influence of infiltration chemistry

Martín Faúndez^{a,c}, Patricia Díaz^a, Gonzalo Riveros^a, Rodrigo Wittwer^a, Francisco Martín^b, Enrique Dalchiele^d, Beatriz Heredia-Cervera^{e,f}, Mahmoud Nabil^e, Gerko Oskam^e, Renan Escalante-Quijano^{e*}, Daniel Ramírez^{a*}

^aLaboratorio de Electroquímica y Nanociencias (LEN), Instituto de Química y Bioquímica, Facultad de Ciencias, Universidad de Valparaíso, Avda. Gran Bretaña 1111, Playa Ancha, Valparaíso, Chile.

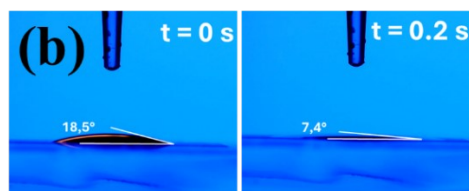
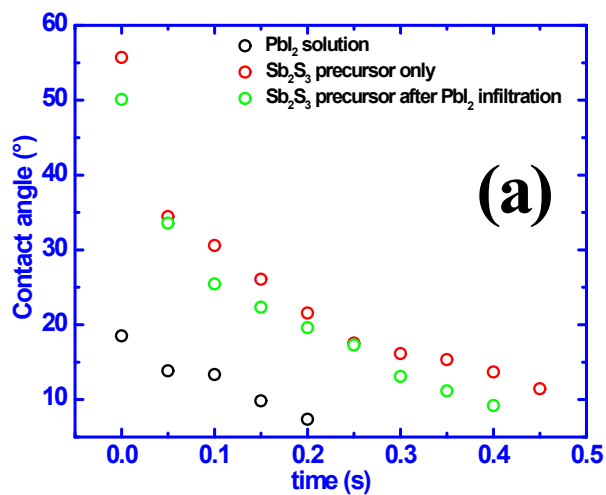
^bInstituto Universitario de Materiales y Nanotecnología, IMANA, Departamento de Ingeniería Química, Universidad de Málaga, E29071 Málaga, Spain

^cDepartamento de Química, Universidad Técnica Federico Santa María, Avda. España 1680, Valparaíso, Chile.

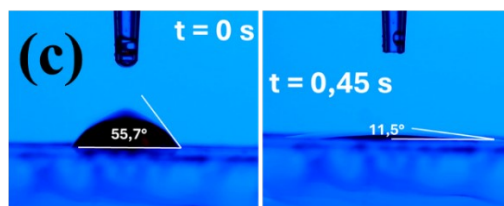
^dFacultad de Ingeniería, Instituto de Física, Universidad de la República, Herrera y Reissig 565, C.C. 30, Montevideo 11000, Uruguay

^eCenter for Nanoscience and Sustainable Technologies (CNATS), Department of Physical, Chemical and Natural Systems, Universidad Pablo de Olavide, 41013 Seville, Spain

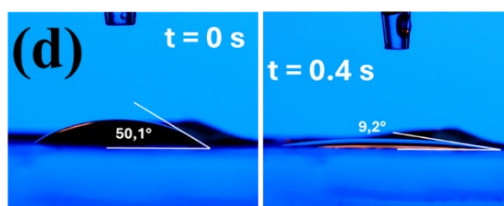
^fDepartment of Applied Physics, CINVESTAV-IPN, Merida 97310 Yucatan, Mexico



5 μL 0.4 M PbI_2
in DMSO at 50°C



5 μL 2 M SbCl_3 + $\text{SC}(\text{NH}_2)_2$ (1:1.8)
in DMF at 50°C



5 μL 2 M SbCl_3 + $\text{SC}(\text{NH}_2)_2$ (1:1.8)
in DMF at 50°C over
previously infiltrated PbI_2

Fig. SM1. Contact angle measurements showing the high infiltration rate using the precursors.

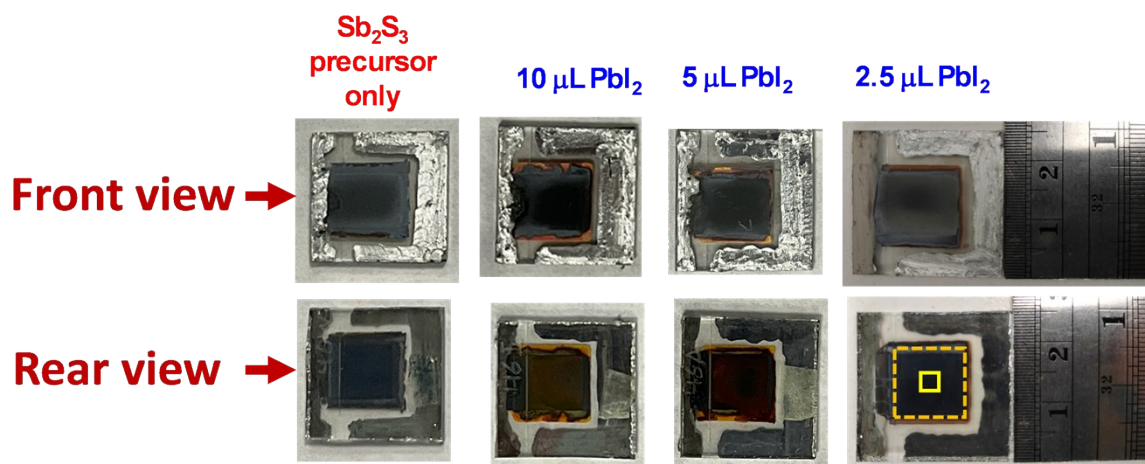


Fig. SM2. Photographs of solar cells. Dashed orange square indicates the infiltration region (active area) and the small yellow square indicates the masked area for characterizations (j - V curves, EIS). Samples were illuminated on the rear side.

Blocking layer effect of c-TiO₂

The spray pyrolyzed c-TiO₂ film was analysed by HR-TEM and cyclic voltammetry. Fig. SM2a,b depicts the feature of c-TiO₂ film which is conformal with the FTO morphology with a thickness near to 30 nm. The blocking layer effect of this film is clearly seen from Fig. SM3c where oxidation of ferrocyanide is fully suppressed and with a small reduction current density wave showing a potential peak shifted more than 400 mV towards more negative potentials compared to the FTO control. This reveals the good covering properties of c-TiO₂ with no defects such as pinholes despite being a very thin film, thus preventing short circuiting in solar cells due to exposing FTO to the photoactive layers after their infiltration and crystallization through the mesoscopic stack.

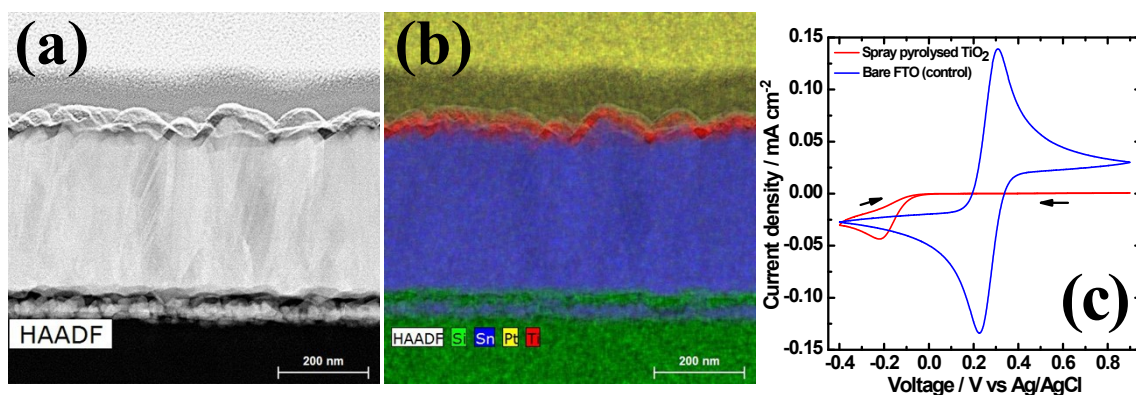


Figure SM3. HR-TEM images of spray pyrolyzed c-TiO₂ on FTO without (a) and with (b) elemental mapping by EDS and its electrochemical activity in aqueous ferri-ferro cyanide from cyclic voltammetry (c). Scan rate: 50 mV s⁻¹.

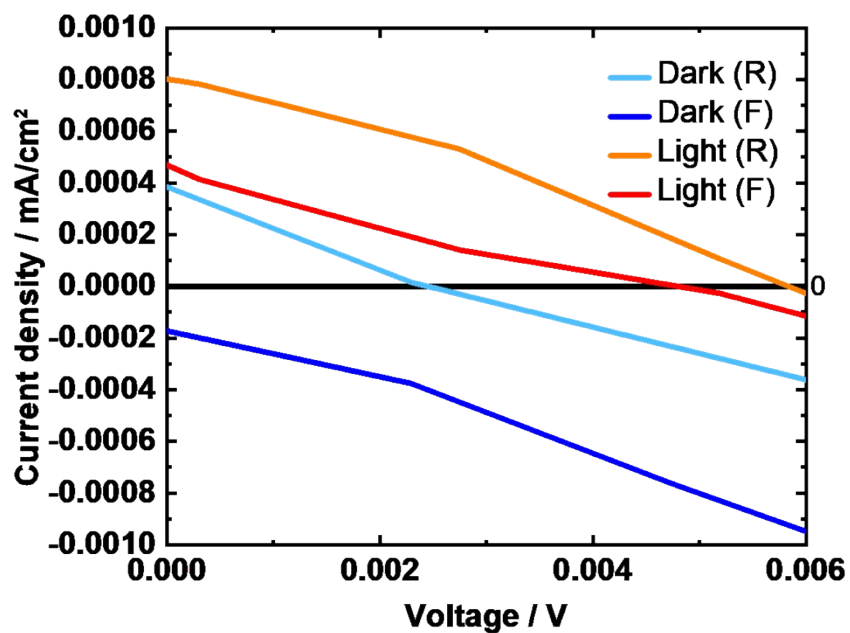


Fig. SM4. j - V typical response (dark vs light) for samples infiltrated with stoichiometric amounts of PbI_2 and Sb_2S_3 precursors to form $\text{Pb}_2\text{SbS}_2\text{I}_3$. F: Forward and R: Reverse voltage bias. The scan rate was 100 mVs^{-1} . Series and parallel resistances (R_s and R_{pa}) were calculated from the derivative of the j - V data (light F/R) at open circuit and short circuit conditions, respectively. R_s : $\sim 6 \text{ k}\Omega \text{ cm}^2$ and R_p : $\sim 1.5 \Omega \text{ cm}^2$.

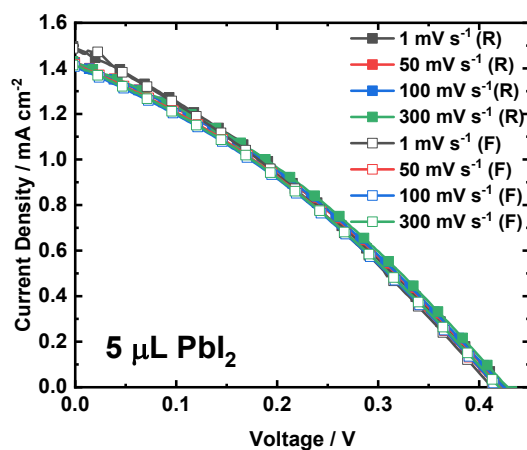
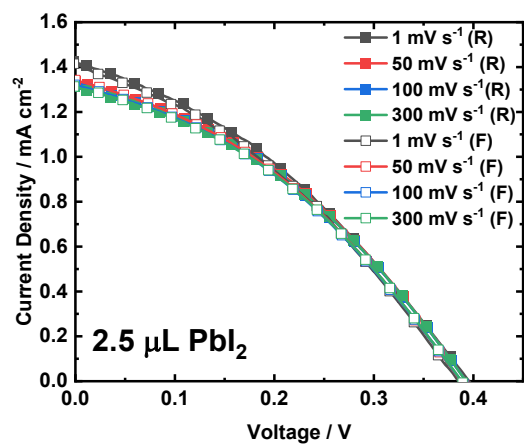
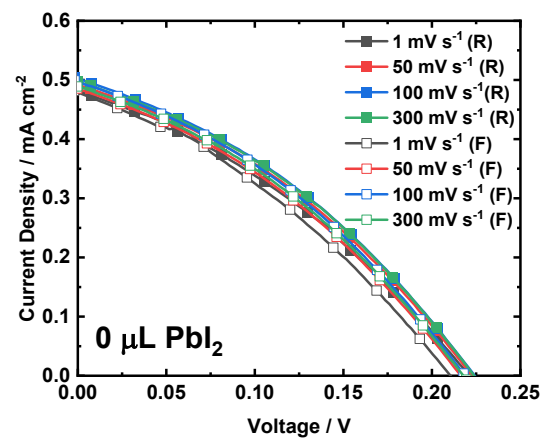


Fig. SM5. Effect of the scan rate over the j - V response for samples infiltrated with 0, 2.5 and 5.0 μL of PbI_2 solution proving the absence of significant hysteresis. F: Forward and R: Reverse voltage bias.

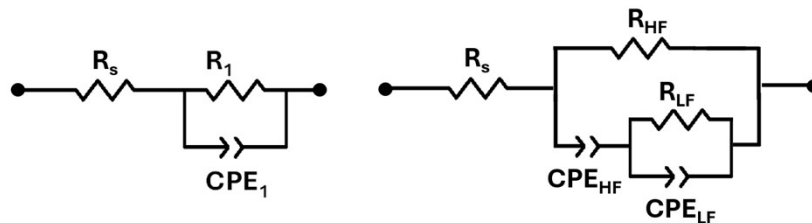


Fig. SM6. Left: Adapted Randles equivalent electric circuit used for fitting EIS data for samples infiltrated with PbI_2 . R is considered a series resistance, whereas R_1 a recombination resistance and CPE_1 a constant phase element used to extract the effective capacitance interpreted as a geometrical capacitance. Right: Nested $R_{\text{LF}}\text{-CPE}_{\text{LF}}$ (LF: low frequency) element connected in parallel to a $R_{\text{HF}}\text{-CPE}_{\text{HF}}$ (HF: high frequency) element used to fit ESI data from samples infiltrated only with the Sb_2S_3 precursor ($0 \mu\text{L PbI}_2$ precursor).

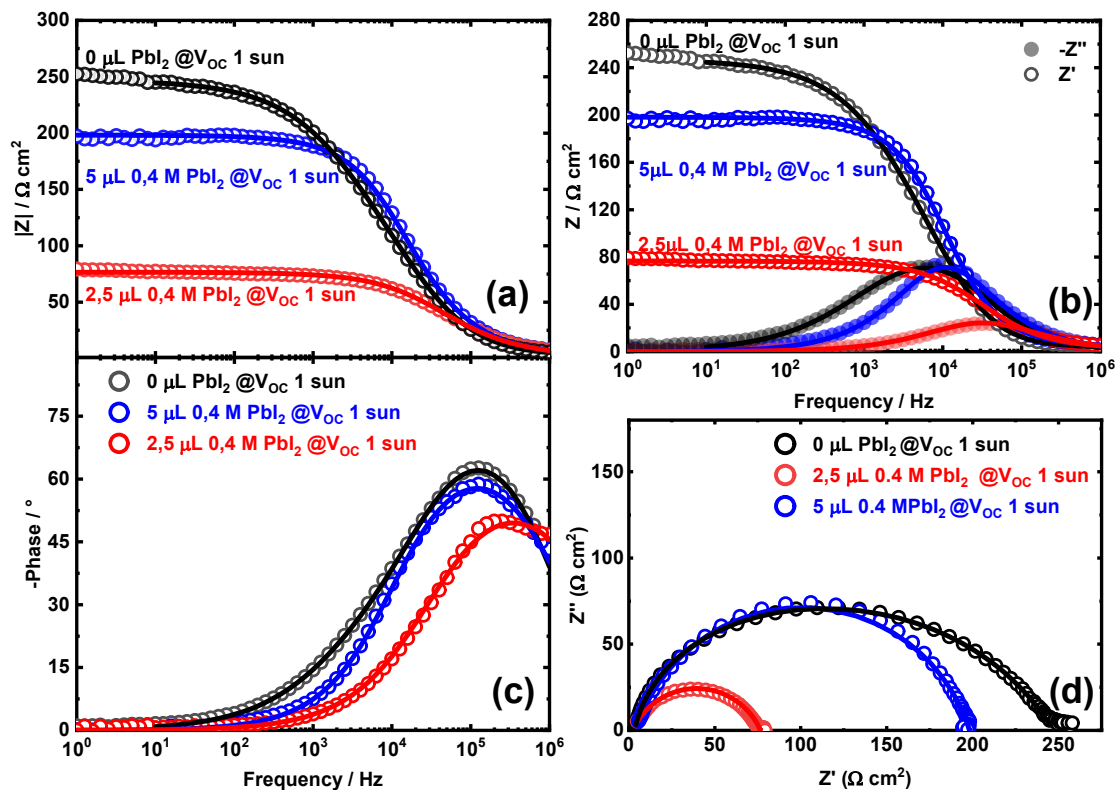


Fig. SM7. Module (a), Cole-Cole, phase (c) and Nyquist (d) diagrams from experimental data, taken at 1 sun and fitted with the “nested” and Randles equivalent electric circuits described in the Fig. SM6 and the main manuscript. Samples prepared by the two-step protocol using 0, 2.5 μL and 5.0 μL are represented by black, red and blue symbols (data) and lines (fit), respectively.